Ultrasonic Inspection During Autoclave Cure of Reflowable-Interface Composite Joints

Tyler B. Hudson[1], Fatimata Baro[2], Austin J. Smith[1], Jin Ho Kang[1], Roberto J. Cano[1], Frank L. Palmieri[1]

[1]*NASA Langley Research Center, Hampton, VA 23681, USA*

[2]*NASA Internships and Fellowships (NIFS), NASA Langley Research Center, Hampton, VA 23681, USA*

In structural bonds, the interface between adherend and adhesive is nearly two-dimensional making the interface susceptible to minute quantities of contamination, which can cause weak bonds. Regulatory organizations such as the Federal Aviation Administration (FAA) often require redundant load paths in secondary-bonded primary-structures due to uncertainty in bond performance. To address this issue, the NASA Convergent Aeronautics Solutions (CAS): Adhesive Free Bonding of Composites (AERoBOND) project is investigating reformulated aerospace epoxy-matrix resins to enable reflow and diffusion of the resin at the joint interface during a secondary bonding and cure process that can eliminate the material discontinuity at the interface. Implementing in-situ process monitoring enables assessing the bond quality during processing rather than waiting for post-fabrication mechanical testing to be completed. In this paper, an in-situ ultrasonic inspection system is used to monitor the joining of three composite laminates assembled using the AERoBOND technique. For each panel, the amplitude of the wave reflection at the joint was measured throughout the cure cycle. The results indicate the timing and extent of reflow and cure of the epoxy resin at the joint. Factors indicating end of cure were ascertained and a metric was developed to qualitatively predict acceptable mode-II fracture toughness based on the ultrasonic amplitude at the joint line during cure. In addition, since the inspection system scans an area of the joint, high-resolution localized results can be obtained across the joint.

I. Nomenclature

AERoBOND = Adhesive Free Bonding of Composites
CAS = Convergent Aeronautics Solutions
ER = Epoxy Rich
ENF = End-Notched Flexure
FAA = Federal Aviation Administration
FEP = Fluorinated Ethylene Propylene
HR = Hardener Rich
RC = Resin Content (wt.%)
LaRC = Langley Research Center
LN_2 = Liquid Nitrogen
UD = Unidirectional

II. Introduction

A. Background and Motivation

In structural bonds, the interface between adherend and adhesive is nearly two-dimensional making the interface susceptible to contamination. Even minute quantities of contamination can cause a weak bond, which results in an inherent uncertainty in adhesive bonds [1]. To meet the certification requirements set forth by regulatory organizations such as the Federal Aviation Administration (FAA), airframe manufacturers often include redundant load paths in

secondary-bonded primary-structures to alleviate the inability to certify bond performance. However, the redundant load paths (e.g., fasteners) tend to be costly and complex to install, add weight to the structure, and degrade the composite components being assembled. In contrast, co-cured composites, although limited in size and complexity, result in predictable structures that are more easily certified for commercial aviation with reduced dependence on redundant load paths [2].

B. AERoBOND Process

As an approach to overcome the issues associated with secondary bonding, the NASA Convergent Aeronautics Solutions (CAS): Adhesive Free Bonding of Composites (AERoBOND) project is investigating reformulated aerospace epoxy-matrix resins to enable reflow and diffusion of the resin at the joint interface during a secondary bonding/cure process. The reflow and intermixing of the matrix resin during assembly can eliminate the material discontinuity at the interface, and thereby remove the dependence of bond performance on adhesion at a nearly two-dimensional boundary. The proposed technology uses a stoichiometric offset of the hardener-to-epoxy ratio on the faying surfaces of laminates. Assembly of the components in a subsequent "secondary-co-cure" process results in a joint with no material discontinuities as illustrated in Fig. 1.

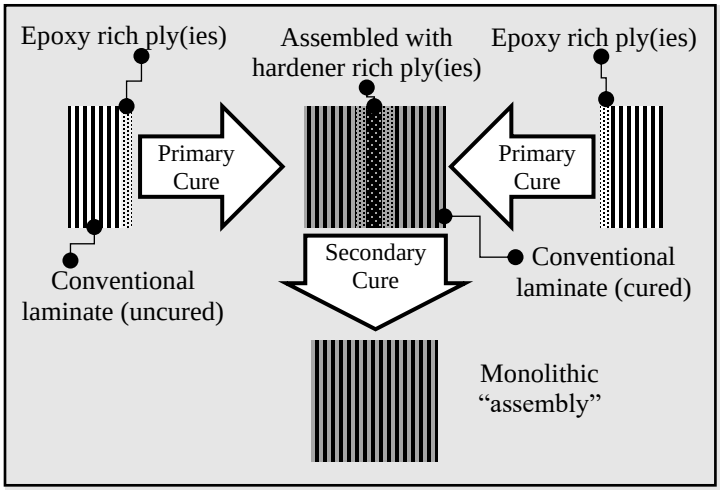

Fig. 1: Schematic of assembly process using offset resin stoichiometry and reinforcing fiber.

Composite components are first prepared with surfaces that are stoichiometrically rich with epoxy functional groups (Fig. 1). During the primary cure, the epoxy rich (ER) resin mixes with the conventional resin; however, the offset stoichiometry in the ER ply(ies) limits the advancement of molecular weight and crosslinking, allowing the resin on the faying surfaces to remain flowable at elevated temperature with intact reactive groups after the primary cure. In the second step, the composite panels are assembled with one or more plies of hardener rich (HR) material between the ER surfaces. During the secondary cure step, the resin in the ER and HR plies intermix and cure to form a composite assembly with no discernable interface, analogous to the interlaminar regions in a conventional laminate. By combining the HR and ER resins, stoichiometric equivalence is achieved, and the molecular weight of the resin can advance until vitrification occurs. AERoBOND process development has evaluated a multitude of parameters including the materials used, the stoichiometric ratio of the epoxy resins, temperature and duration of cure cycles, and relative ply thickness of ER and HR plies, and resulting mechanical properties [3], [4]. However, without in-situ process monitoring, the condition of the AERoBOND joint test article was unknown until post-fabrication inspection and mechanical testing.

C. Alternative Methods

There has been very little work investigating reflowable interfaces for bonding composites. McAdams et al. filed a patent for FusePly™* technology marketed by Solvay® [5]. The chemistry of FusePly™ is not disclosed, but the

* *Specific vendor and manufacturer names are explicitly mentioned only to accurately describe the hardware used in this study. The use of vendor and manufacturer names does not imply an endorsement by the U.S. Government nor does it imply that the specified equipment is the best available.*

patent indicates that it uses an epoxy resin with off-set stoichiometry such that residual reactive sites (either epoxy or hardener) remain in the resin after a full autoclave cure cycle is complete. The material is applied to bonding surfaces in the form of a wet peel ply. Once the cure peel ply is removed, the site is ready for bonding. In the case of FusePly™, the resin layer left behind after peeling may have residual reactivity to enhance bonding, but resin reflow is likely not possible due to the assumed high degree of cure [6].

D. Ultrasonic Inspection During Cure

Prior work by this research group demonstrated ultrasonic inspection as a method to determine gelation and vitrification of resin and for detecting void defects across an area of a composite panel during cure. The inspection system operates by using a raster scanner and ultrasonic transducer to send and receive ultrasonic acoustic waves at continuous intervals over a defined area throughout cure. The inspection system was designed to operate inside the high-temperature and high-pressure environment of an oven and/or autoclave [7]-[9]. Numerous factors can affect the quality of cure such as material variability (e.g., cure kinetics, fiber volume fraction, defects, etc.), temperature, and pressure. Additional studies on the effect of cure cycle can be found in [10]-[13].

E. Objective

This work investigated the use of the in-situ ultrasonic inspection system to monitor the joining of three composite panels (six "half" panels) assembled using the AERoBOND technique during secondary cure. Two sets of composite panels were joined with unidirectional HR prepreg and the third with fabric HR prepreg in the joint.

III. Experimentation

F. Composite Panel Fabrication

Five bonded composite panels (Size: 305 mm × 152 mm) denoted as 1A, 1B, 2A, 2B and 3A, were fabricated and tested using the end-notched flexure (ENF) test method (ASTM D7905/D7905M) to measure mode-II (shear) fracture toughness [14], [15]. Hexcel® HexPly™ IM7G/8552 was utilized as the conventional prepreg material. 1A and 1B were identical panels with unidirectional (UD) HR prepreg at the joint. Similarly, panels 2A and 2B were identical panels with UD HR prepreg at the joint, but with a shortened duration between primary and secondary cure as compared to 1A and 1B. Panel 3A had fabric HR prepreg in the joint. Panels denoted with an "A" (panels 1A, 2A, and 3A) were ultrasonically inspected during secondary cure and "B"-panels (panels 1B and 2B) served as the control group to ensure the inspection did not significantly change the mode-II fracture toughness of the joint (e.g.,1A vs. 1B and 2A vs. 2B). A control panel was not fabricated for panel 3. The ER and HR material had an initial stoichiometric offset of r = 0.15 and 2.5 [Eq. (1)], respectively.

$$r = \frac{eq_H}{eq_E} \equiv \frac{molar\ equivalents\ of\ hardener}{molar\ equivalents\ of\ epoxy} \tag{1}$$

Previous work using rheology and calorimetry indicated an ER r-value of less than or equal to 0.15 prevented gelation during primary cure. The resins were formulated using API-60® (part A) epoxy resin supplied by Kaneka North America® with an epoxy equivalent weight of 131 g/mol and diethyltoluenediamine (DETDA) (part B) hardener supplied by Alfa Chemistry®. Unidirectional tape was fabricated using an in-house prepreg machine at NASA Langley Research Center (LaRC) to impregnate the ER and HR resins into Hexcel® IM7/G 12K fiber. For primary cure, "half" panels were laid up in a vacuum bag where one of the half panels had nine plies of IM7G/8552 (Hexcel® HexPly™) and two plies of ER prepreg, and the other had ten plies of IM7G/8552 and two plies of ER prepreg. The offset of one ply of IM7G/8552 between the half panels ensured the crack starter was at the middle of the panel for ENF testing. For panels 1A and 1B, the primary cure cycle was as follows: apply vacuum to the bag, heat to 107°C (225°F), apply 689 kPa gauge pressure (100 psig), hold 2 hours, heat to 177°C (350°F), hold 0.75 hour. For panels 2A, 2B, and 3A, the first hold time was extended to 3 hours. Following primary cure, the half panels of Panels 1A, 1B, 2A, and 2B were assembled with two plies of unidirectional HR prepreg. For Panel 3A, the half panels were combined with one ply of fabric HR prepreg (also manufactured using LaRC's in-house prepreg machine). For all panels, a 102 mm × 152 mm × 13 μm fluorinated ethylene propylene (FEP) crack starter film was placed on one edge between the HR prepreg and the half panel with ten plies of IM7G/8552 to create the crack starter for ENF testing (Fig. 2). The secondary cure cycle was as follows: apply vacuum, heat to 107°C (225°F), apply 689 kPa gauge pressure (100 psig),

hold 1 hour, heat to 177°C (350°F), hold 4 hours. This two-step fabrication approach is illustrated conceptually in Fig. 1.

The primary and secondary cure cycles for panels 1A and 1B were separated by over seven months (Mar. 2020 and Oct. 2020, respectively) because of mandatory telework requirements at LaRC due to COVID-19. The half panels fabricated during primary cure were stored at room temperature prior to the secondary cure (the HR prepreg was fabricated in Jan. 2020 and stored in freezer). Because of the prolonged time between process cycles, the expectation was that mechanical properties would be adversely affected; however, testing was conducted to demonstrate the inspection system and quantify the effect on fracture toughness. The rest of the panels did not experience an extended time gap between primary and secondary cure. The presupposition was the panels (2A, 2B, and 3A) with a shorter time gap between primary and secondary cure would perform better than 1A and 1B. A summary of the test parameters from the different configurations is presented in Table 1.

Table 1: Panel materials and processing conditions.

	Panel				
	1A	1B	2A	2B	3A
Test Factor	**Material and Layup Parameters**				
ER r-value	0.15	0.15	0.15	0.15	0.15
ER RC	62-69%	62-69%	62-67%	62-67%	62-67%
ER fiber	UD	UD	UD	UD	UD
ER # of plies per half panel	2	2	2	2	2
HR r-value	2.5	2.5	2.5	2.5	2.5
HR RC	68-76%	68-76%	48-50%	48-50%	42-49%
HR fiber	UD	UD	UD	UD	Carbon Fabric
HR # of plies	2	2	2	2	1
Cured Panel Thickness (mm)	4.88	5.05	4.37	4.34	4.50
	Cure Cycle Parameters				
Time between primary cure and secondary cure (weeks)	28	28	5	5	0.7
Primary hold 1 (min)	120	120	180	180	180
Primary hold 1 (°C)	107	107	107	107	107
Primary hold 2 (min)	45	45	45	45	45
Primary hold 2 (°C)	177	177	177	177	177
Secondary hold 1 (min)	60	60	60	60	60
Secondary hold 1 (°C)	107	107	107	107	107
Secondary hold 2 (min)	240	240	240	240	240
Secondary hold 2 (°C)	177	177	177	177	177
Ramp rate (°C/min)	2.8	2.8	2.8	2.8	2.8

G. Inspection During Secondary Cure

A MISTRAS® motorized X-Y raster scanner with a high-temperature contact transducer (Olympus® X2002, 2.25 MHz center frequency) was utilized to perform ultrasonic scans during the secondary cure cycle. The vacuum bag was sealed to the top of the composite panel exposing an area for inspection. By sealing the vacuum bag to the already cured top half panel, pressure was applied to the joint line. A thin layer of ultrasonic couplant (Echo Ultrasonics® Glycerin) was placed between the transducer and the composite panel (Fig. 2).

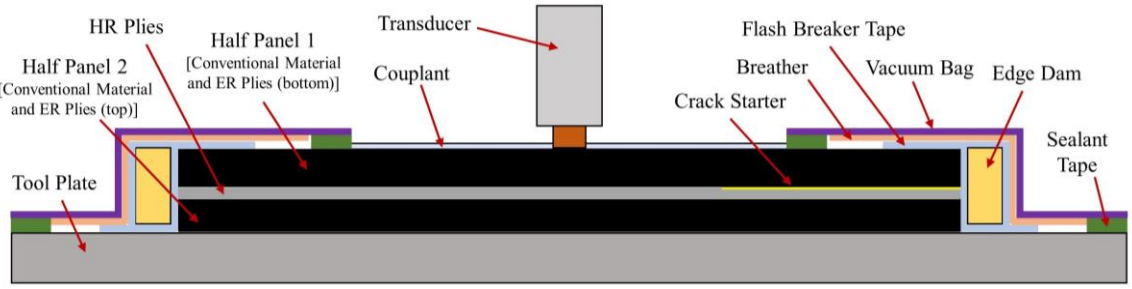

Fig. 2: Arrangement of composite panel, vacuum bag, and ultrasonic transducer.

The X-Y raster scanner was mounted inside an unsealed cooling enclosure made of porous ceramic insulation boards (Skamol® Skamotec™ 225). The scanner utilized a cantilever scanning arm protruding out of the cooling container through a slot to control the location of the transducer. The enclosure was periodically cooled using a liquid nitrogen (LN_2) delivery system. When the internal temperature of the enclosure reached 34°C (93°F), LN_2 was delivered to the unsealed enclosure by opening a cryogenic solenoid valve that connected the enclosure to a LN_2-filled Dewar tank located outside the autoclave. The temperature controller was programmed to close the valve, stopping flow of LN_2, immediately upon registering a decrease in temperature. The cooling system ensured that the scanner motors did not exceed their maximum desired operating temperature of 38°C (100°F). A photograph of the experimental setup inside the autoclave is shown in Fig. 3.

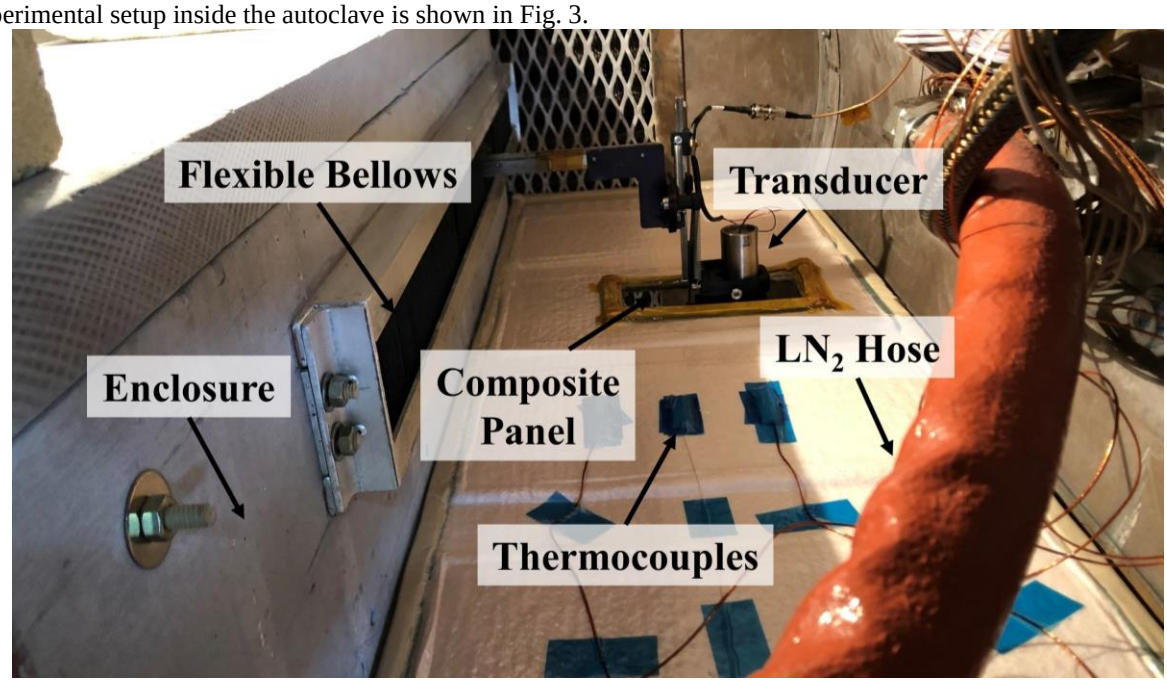

Fig. 3: Photograph of experimental setup prior to secondary cure (Image Credit: NASA).

A MISTRAS® Remote Ultrasonic Testing (UT) System was used to operate the motion-control motors and generate/record the ultrasonic waves during the scanning process. The scan speed in each direction was 36 mm/s with a 1 mm × 1 mm per pixel resolution with 100 measurements averaged at each point. The average scan time was 53 s for the 114 mm × 25 mm scanning area for panel 1A. For panels 2A and 3A, the scanning area was 89 mm × 19 mm. Only "A"-panels were scanned. "B"-panels were cured according to identical processing conditions to evaluate whether the scanning process affected the mechanical properties. The sampling rate was 100 MHz. A digital high pass filter of 0.5 MHz and a low pass filter of 12.5 MHz was applied during signal acquisition. C-scan and B-scan images were generated in real-time. The C-scan images, in this work, display the maximum amplitude of the reflections from the joint line, denoted by gate 4. The B-scans are cross-sectional images through the thickness of the composite panel. One scan was performed prior to cure and then repeated throughout the cure cycle. The temperature of the panels was quantified using thermocouples throughout cure. In addition to the scans performed during cure, the composite panels

were ultrasonically inspected after final cure prior to machining, and each ENF test specimen was again ultrasonically inspected post machining prior to testing.

H. Mechanical Testing

Six specimens (size: 203 mm × 20 mm) were cut from each panel using a water jet. ENF testing was conducted using a 3-point bend fixture (Fig. 4) according to ASTM D7905-14 to measure mode-II fracture toughness using six replicate specimens from each panel [14], [15]. The sides of the specimen were painted white for visualization of the crack extension.

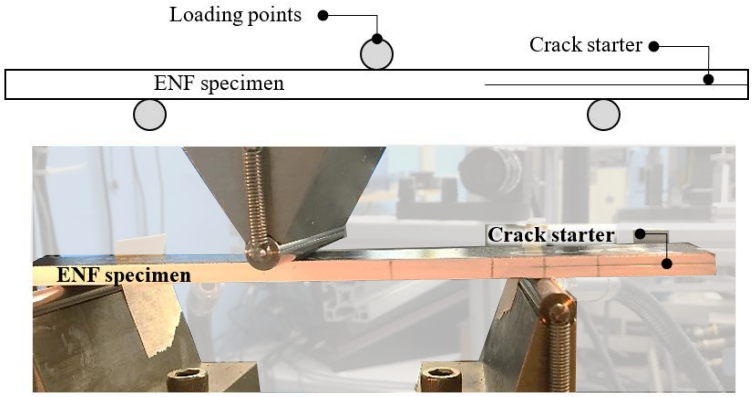

Fig. 4: Specimen schematic and a photograph of test setup for the ENF test.

IV. Results and Discussion

A. Ultrasonic Inspections

For each panel and scan, time gates were setup in the ultrasonic waveforms to calculate the maximum absolute amplitude of the reflection at the joint line (Fig. 5). The maximum absolute amplitude within each time gate was calculated at every location and the result assigned to that location. For example, during scan 67 (just prior to cooldown) for Panel 2A at location x = 44 mm and y = 10 mm, the maximum absolute amplitude at the joint line (gate 4) was 0.32 (32%) (Fig. 5).

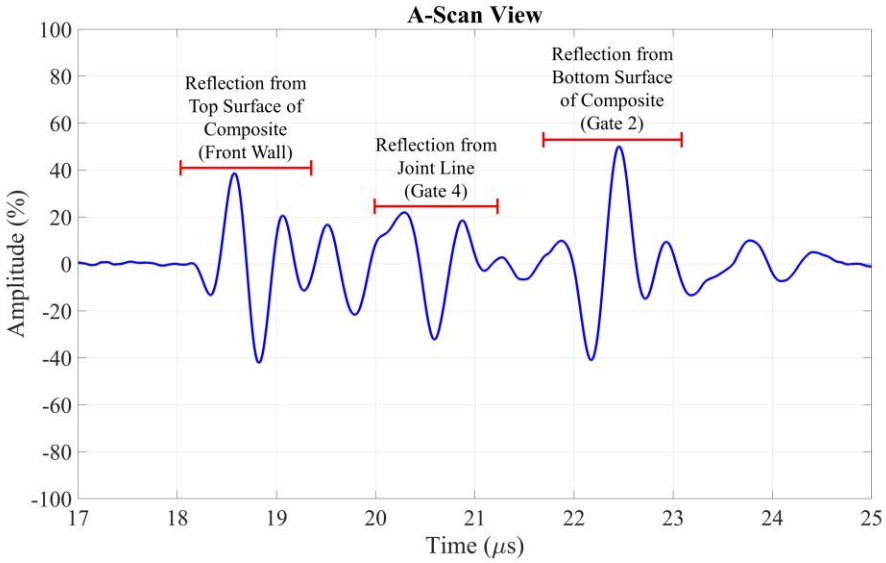

Fig. 5: A-scan waveform from Panel 2A at location x = 44 mm and y = 10 mm (Cursor location in Fig. 6) during scan 67 (just prior to cooldown).

For Panel 2A, 90 scans of the inspection area were performed throughout the cure cycle. A C-scan image/map (top view) of the maximum amplitude within this time gate is shown for the last scan prior to cool down in Fig. 6 and a montage image of a subset of scans during and after cure is shown in Fig. 7. The starting time of each scan and the temperature of the composite panel are listed in Fig. 7. The cursor in Fig. 6 indicates the location of the A-scan waveform in Fig. 5 and the location along the y-axis for the B-scans in Fig. 8 and Fig. 9.

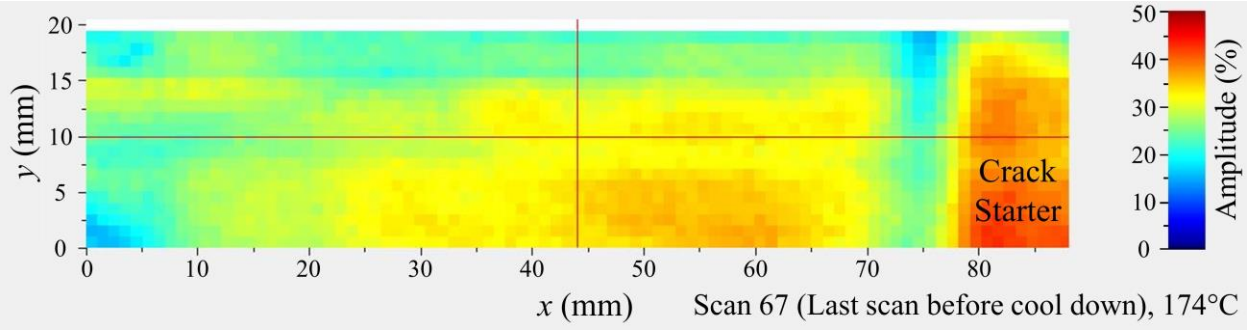

Fig. 6: Panel 2A C-scan image of the maximum amplitude measured at the AERoBOND joint line during the last scan before cooldown (Scan 67).

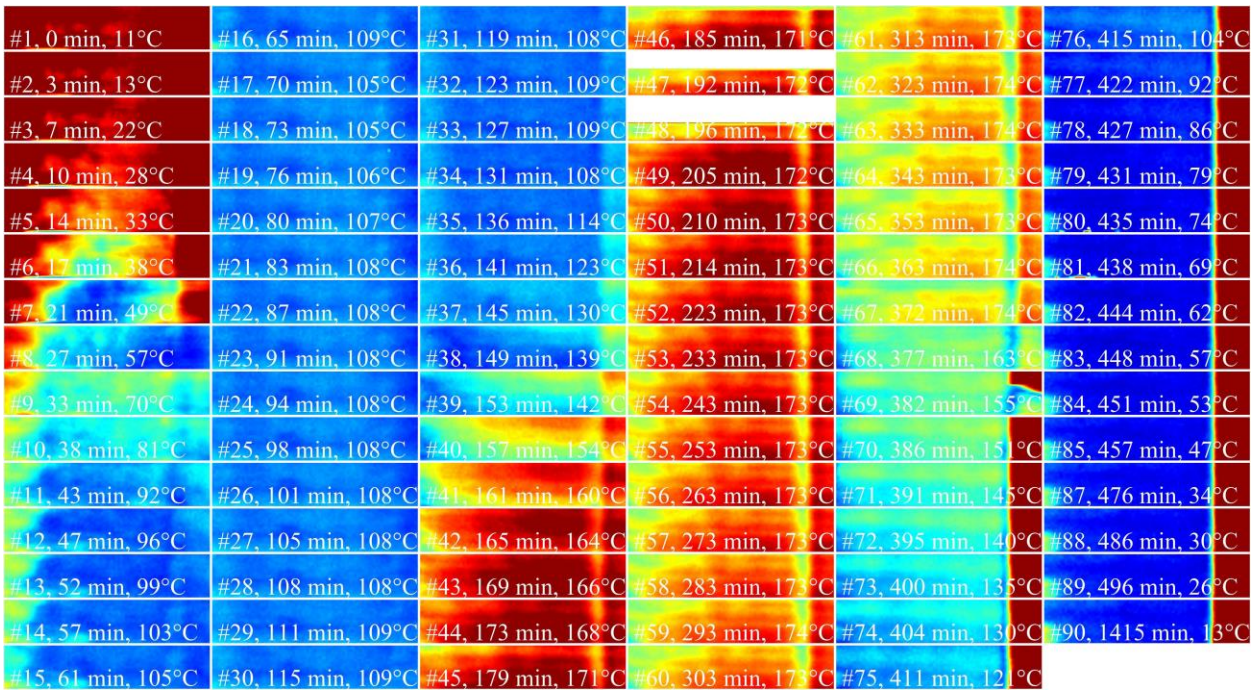

Fig. 7: Panel 2A C-scan images of the maximum amplitude measured at the AERoBOND joint line throughout the cure cycle.

The B-scan (cross-sectional slice) from the final inspection is shown in Fig. 8, which was performed the following day. The crack starter was fully visible. Reflections from the joint line were minimal and there were little to no voids at the joint, which is an indication of a high-quality bond that would be expected to exhibit good mechanical strength [16]. A montage of B-scan images taken throughout cure in shown in Fig. 9.

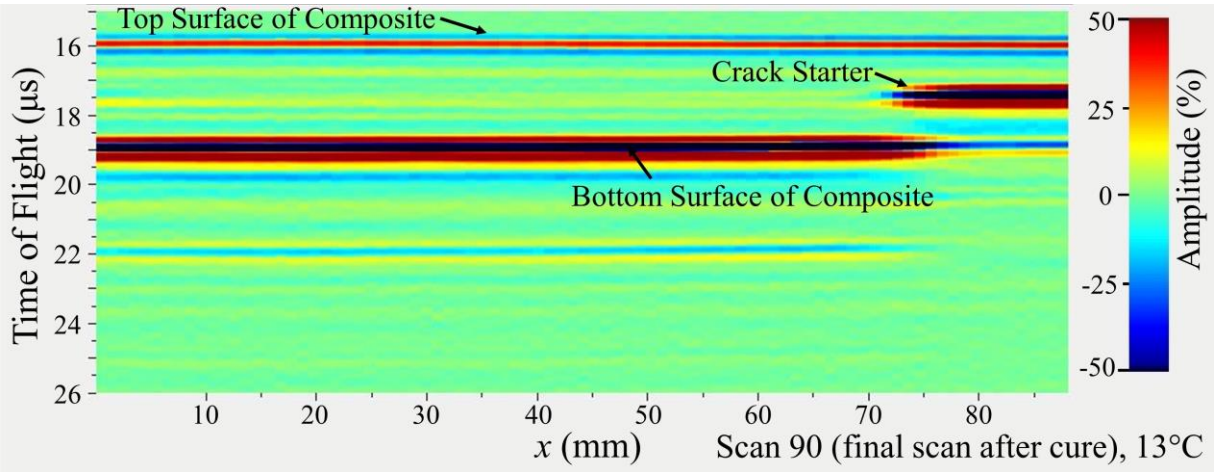

Fig. 8: B-scan image of scan 90 (final scan after cure) of Panel 2A.

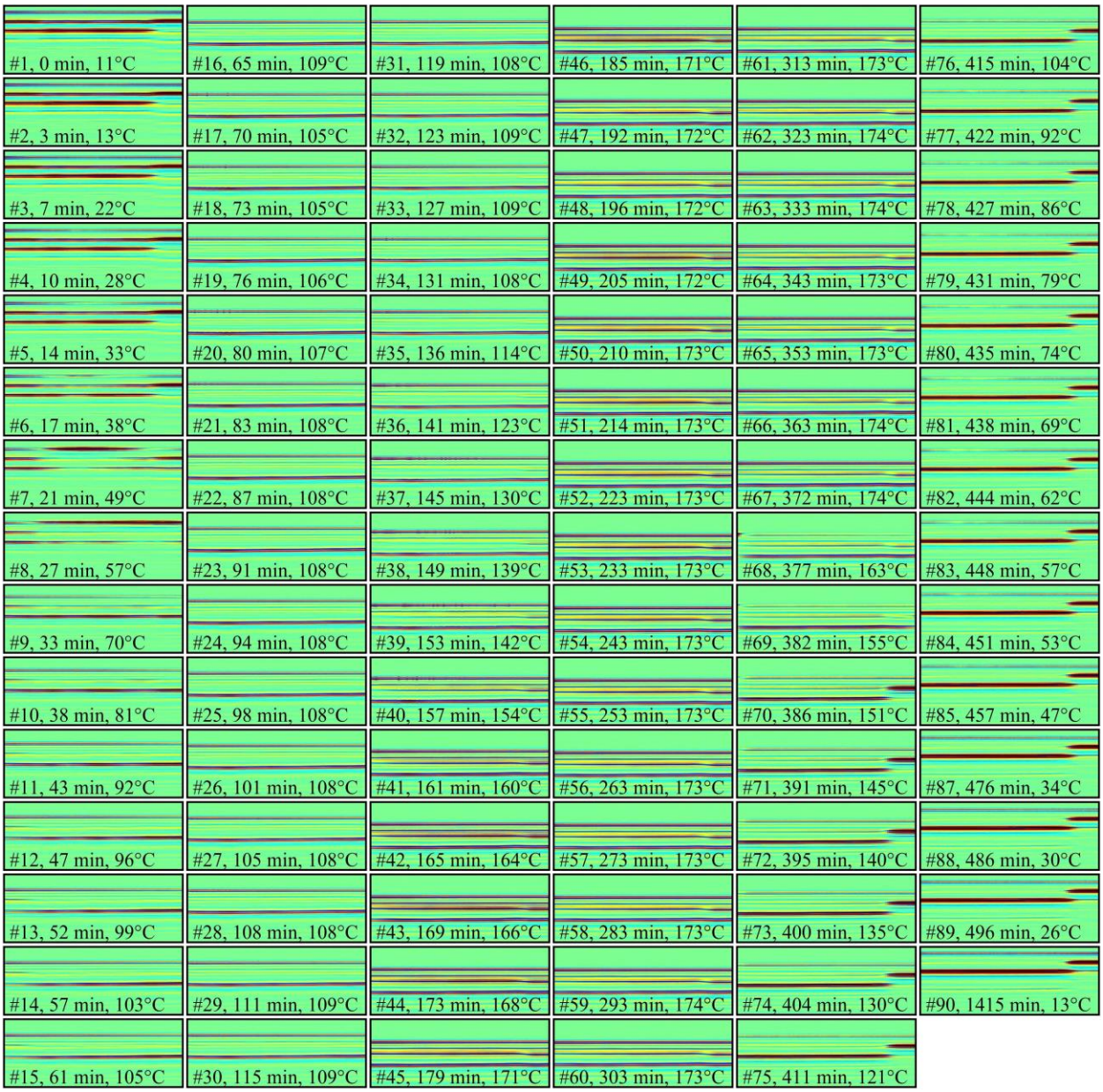

Fig. 9: B-scan images at one *y*-location (*y* = 10 mm) throughout the cure cycle for Panel 2A.

For this configuration (2A), there were high reflections at the joint in the first period of time in both the C-scans and B-scans (scans 1-7, 0-21 min). As temperature rose, the crack starter vanished and the reflections observed at the center of the B-scans diminished (scan 8-31, 27-119 min), which corresponded to the flow of ER and HR coming into contact with the FEP film insert. With liquid resin wetting both sides of the FEP film insert, the ultrasonic wave passed through the film with minimal reflection. During the second temperature ramp, there was a marked increase in the joint line reflections (scan 36-42, 141-165 min). At near constant temperature during the second temperature hold, (scan 43-67,169-372 min), the joint line reflections decreased, and the crack starter again became visible. This decrease in joint line reflections was a result of reduced acoustic impedance mismatch between the adherends and the joint, which corresponded to stochiometric equivalence having been achieved (i.e., ER and HR resins having mixed) and cure of the joint line occurring.

Cooldown began after scan 67 and prior to scan 68. The pressure was also vented from the autoclave after scan 67. Cooldown resulted in a reduction of reflections from the joint and led to a clear visibility of the crack starter. In Fig. 7, the white area at the top of scans 47 and 48 represents missing data during these two scans.

Montage images of both the B-scans and C-scans of the maximum amplitude from the joint line are included in Fig. 12-Fig. 15 in the appendix. During the cure cycle for Panel 3A, there was an equipment malfunction at ~190 minutes that prevented full area C-scans from being collected. B-scans at a single *y* location were restored at ~230 minutes and C-scans across half the area were resumed at ~420 minutes. Despite the malfunction, the average amplitude was able to be determined from the reduced data for comparison with Panel 1A and 2A.

B. Ultrasonic Data Analysis

1. *Average Amplitude at Joint Line*

An average amplitude value of each C-scan image was generated using MATLAB®. Each value corresponds to the average amplitude of pixels in a scan image excluding the area over the crack starter. The range is from 0 to 1 (100%). The average amplitude of each scan is plotted along with temperature against time for panels 1A, 2A, and 3A (Fig. 10).

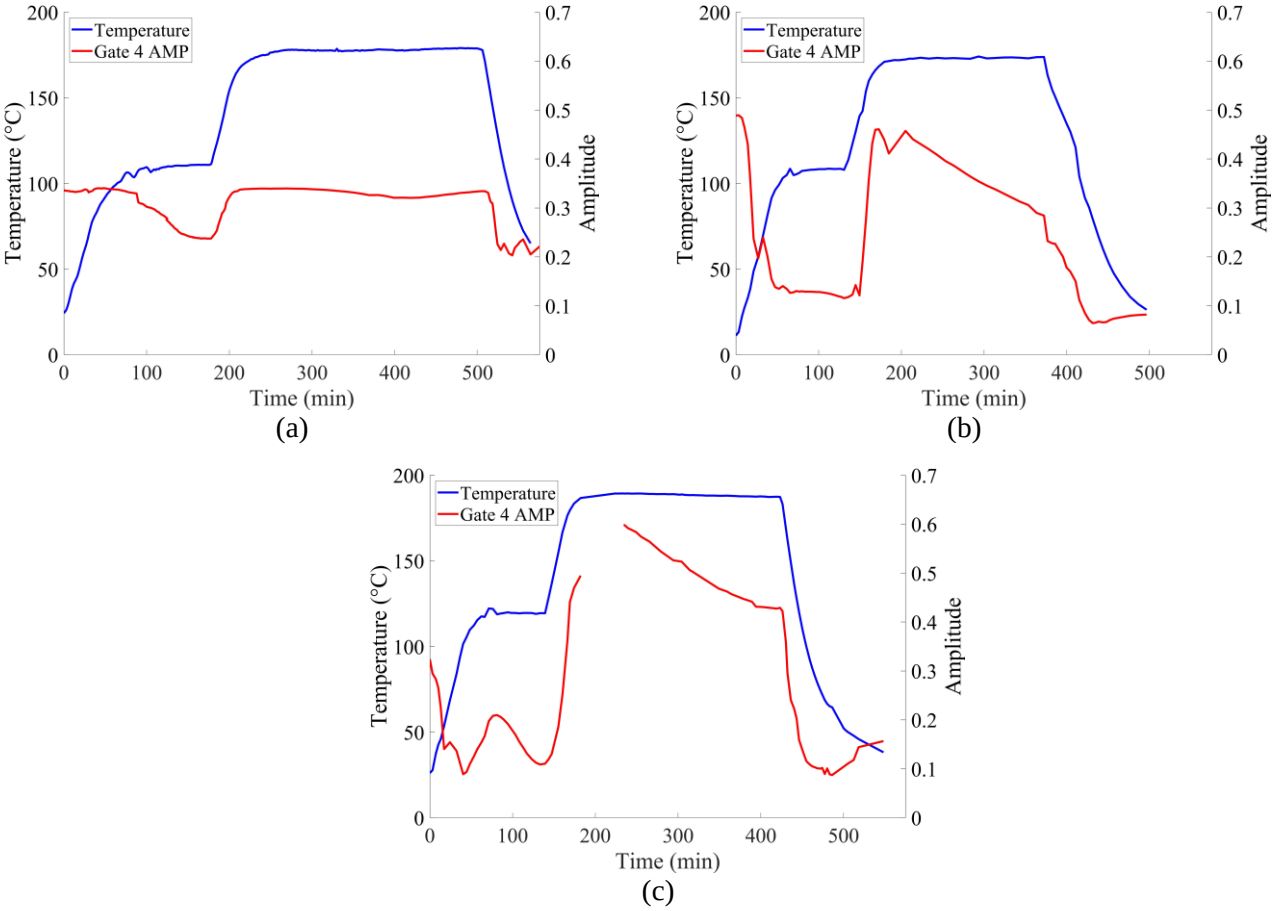

Fig. 10: Change in temperature and amplitude from the joint line (excluding crack starter area) during the cure cycle for Panel 1A (a), Panel 2A (b), and for Panel 3A (c).

For all three experiments, an inverse behavior of the joint line amplitude compared to the temperature in the beginning of the cure cycle, as shown in Fig. 10. This inverse behavior is attributed to the decrease of the resin viscosity as the temperature increased. During the second temperature ramp, the amplitude increased significantly as the temperature rose, especially for Panel 2A and 3A (~150-200 min). As mentioned, for Panel 3A, the gap in the data (~190-230 min) was due to an equipment malfunction and an absence of C-scans during this time interval. The scanner was able to be reset and inspections continued through the remainder of the experiment. During the secondary temperature hold [~177°C (~350°F)], there was only a small decrease in the amplitude of joint line reflections for Panel 1A compared to Panels 2A and 3A. In addition, the joint line amplitude decreased throughout the second temperature hold for both panels 2A and 3A and did not level off as with Panel 1A. For Panel 1A, this difference in amplitude throughout the cure cycle is indicative of poor reflow and diffusion of the ER and HR resins. One reason

for this was that the primary and secondary cures for Panel 1A were separated by 28 weeks due to delays in testing resulting from the Covid-19 pandemic. The two adherends with ER surfaces were stored at room temperature and the HR prepreg was in the freezer. As for Panel 2A and 3A, the continuous decrease in amplitude throughout the second temperature hold points to sufficient intermixing of the ER and HR resins and that cure was occurring in the joint even at the beginning of cooldown. The reduction in joint line amplitude corresponds to the properties of the joint approaching the properties of the surrounding laminate. It is hypothesized that if the second temperature hold for Panels 2A and 3A were extended, cure would have continued and eventually the joint line amplitude would have leveled off. This was observed as an initial drop in the joint line (gate 4) amplitude during the first 177°C (350°F) hold during a temperature calibration experiment performed on the already-cured Panel 2A (Fig. 11b). Extending the second temperature hold could have enhanced the mechanical properties of these panels.

2. Temperature Calibration (Panel 2A)

Temperature calibration of the ultrasonic amplitude was also studied using Panel 2A by thermally cycling the already cured laminate. A summary of the results obtained is shown in Fig. 11.

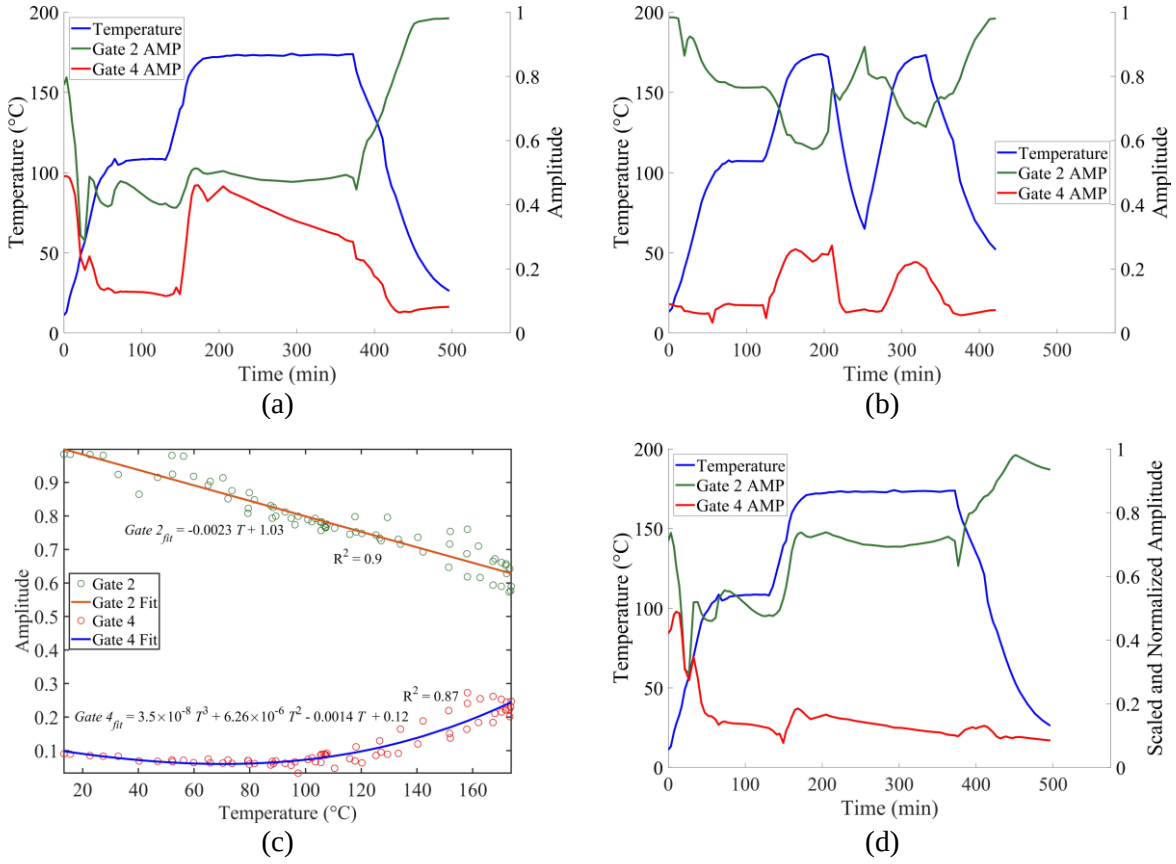

Fig. 11: For panel 2A, (a) change in amplitude and temperature during secondary cure; (b) change in amplitude and temperature during temperature calibration cycle for the already-cured panel 2A; (c) amplitude versus temperature during temperature calibration; (d) scaled amplitude and temperature during secondary cure.

The temperature calibration experiment studied the effect of temperature on the amplitude from the joint line (gate 4) and backwall (gate 2) by measuring the ultrasonic amplitude during a subsequent temperature cycle on the already cured Panel 2A (Fig. 11b). The ultrasonic amplitude versus temperature from the temperature calibration experiment is plotted in Fig. 11c. The amplitude of gate 2 (backwall) has a linear inverse relationship compared to the temperature across the entire temperature range (i.e., as temperature increases, amplitude decreases and vice versa). The fit equation in Fig. 11c for the joint line (gate 4) is an n=2-degree polynomial, which shows an increase in gate 4

amplitude beginning at ~90°C (194°F). These fit equations along with a scaling function were used to generate Fig. 11d where the amplitude was scaled (Eq. 2) and normalized (Eq. 3).

$$A_{scaled}(t,T) = \frac{A_{exp}(t)}{A_{fit}(T)} \quad (2)$$

$$A_{norm}(t,T) = A_{scaled}(t,T) \times \frac{\max(A_{exp})}{\max(A_{scaled})} \quad (3)$$

Where:
$A_{exp}(t)$: Experimental amplitude at time, t.
$A_{fit}(T)$: Amplitude obtained from the fit function of Panel 2A temperature calibration at temperature, T.
$A_{scaled}(t,T)$: Scaled amplitude.
$A_{norm}(t,T)$: Normalized, scaled amplitude.

Equation (1) removes the temperature effects on the ultrasonic amplitude during the cure cycle while equation (2) normalizes the data to the same maximum value as the unscaled, experimental data. Fig. 11(d) shows that the scaled and normalized amplitude of the joint line (gate 4) continuously decreased for almost the entire cure cycle and the backwall (gate 2) amplitude increased for the majority of the cure cycle. There are several key takeaways from these figures. Panel 2A has a higher chance of succeeding during mechanical testing because its joint amplitude continuously decreased and the backwall amplitude continuously increased when temperature effects were excluded. This corresponds to its joint properties becoming equivalent to the properties of the surrounding laminate, and therefore presenting minimal reflections at the end of cure.

C. Mechanical Testing

Of the panels fabricated and studied in this work, panels 2A, 2B, and 3A produced satisfactory mode-II fracture toughness as measured using the ENF test method. For panels 2A and 2B, the average mode-II fracture toughness was 108% and 110% of the co-cured baseline toughness, respectively, when tested in the non-precracked (NPC) condition. For both Panel 2A and 2B, the mode-II fracture toughness was 75% of the co-cured baseline when tested in the precracked (PC) condition. Although both ENF-NPC and ENF-PC results of Panel 3A were high, the mechanical test performance of Panel 3A cannot be reported quantitatively per the ASTM standard because of invalid crack front variability. For Panel 1A and 1B, the average mode-II fracture toughness was only 32% of the co-cured baseline. In addition, the crack advanced in four of the twelve mechanical test samples (two from each panel) during water jet machining rendering those specimens invalid. Another two specimens were outside of the thickness variation tolerance specified by the test standard, which causes asymmetric loading. The crack front did not advance during machining for any of the samples from panels 2A, 2B, and 3A. The weakened performance of 1A and 1B is related to the unplanned aging of the precursor materials. They were fabricated prior to mandatory telework at LaRC due to Covid-19 in March 2020. The half panels were stored at room temperature for over seven months prior to the secondary cure (the HR prepreg was fabricated in Jan. 2020 and stored in a freezer).

From these results, there appears to be no negative impact on mode-II fracture toughness resulting from the in-situ inspection during secondary cure (Panel 1A vs. Panel 1B and Panel 2A vs. 2B). In addition, the ultrasonic data recorded and analyzed from Panels 1A, 2A, and 3A indicates that by monitoring the joint line reflections during secondary cure, the potential success or failure of the panels during mechanical testing could be predicted. The mechanical testing results are summarized in Table 2.

Table 2: Mechanical testing results of the different composite panels.

	Panels				
Test Factor /Result	1A	1B	2A	2B	3A
ENF-NPC	32%	32%	108%	110%	High value, invalid crack front
ENF-PC	-	-	75%	75.1%	High value, invalid crack front
Qualitative Assessment	Weak	Weak	Tough	Tough	Tough

V. Summary and Conclusions

AERoBOND is a new joining approach using reformulated epoxy matrix resin components to obtain improved aerospace composite joints. Ultrasonic inspection scanning was integrated into the autoclave to monitor the curing process in real time. Ultrasonic inspections of AERoBOND joints were performed at continuous intervals (approximately every two minutes) for the entirety of the autoclave process cycle. By using the recently developed in-situ inspection system with a mobile ultrasonic transducer, localized results across a large area of the joint were obtained with fine resolution. The wave reflections at the joint interface were measured and quantified. From these results, a determination was made on the timing of flow of the ER/HR resin, cure of the joint line was monitored, and the propagation of the crack at the film insert during cool down was observed. Joint line amplitude data collected using the in-situ inspection system during secondary cure was analyzed and correlated with the success or failure of the AERoBOND configuration (materials, layup, and processing conditions). For panels with high mode-II fracture toughness, the joint line amplitude continuously decreased over time during the second temperature hold (and throughout the entire cure cycle when temperature effects were removed) indicating its material properties were approaching that of the surrounding laminate. In addition, based on the results presented in this paper, a framework was discussed for adjusting the cure cycle based on feedback from the in-situ inspection system to optimize bond performance.

VI. Acknowledgments

The authors thank Sean Britton, Hoa Luong, and Wilfredo Flores from the NASA Langley Research Center who were instrumental in the fabrication of the composite panels.

VII. References

[1] Palmieri, F.L., Ledesma, R., Fulton, T., Arthur, A., Eldridge, K., Thibeault, S., Lin, Y., Wohl, C. J. and Connell, J.W., "Picosecond pulsed laser ablation for the surface preparation of epoxy composites," *SAMPE Technical Conference Proceedings*, Seattle, WA, May 22-25, 2017. https://ntrs.nasa.gov/citations/20170006187

[2] Fuertes, T. A. S., Kruse, T., Koerwien, T. and Geistbeck, M., "Bonding of CFRP primary aerospace structures – discussion of the certification boundary conditions and related technology fields addressing the needs for development," *Composite Interfaces*, Vol. 22(8), pp. 795-808, 2014. https://doi.org/10.1080/09276440.2015.1077048

[3] Palmieri, F.L., Hudson, T.B., Smith, A.J., Cano, R.J., Kang, H.J., and Lin, Y., "Latent cure epoxy resins for reliable joints in secondary-bonded composite structures," *Composites Part B: Engineering*, Vol. 231, 109603, 2022. https://doi.org/10.1016/j.compositesb.2021.109603

[4] Smith, A.J., Salem, J.A., Hudson, T.B., and Palmieri, F.L., "Interlaminar mechanical performance of latent-cure epoxy joints," *Composites Part B: Engineering*, Vol. 255, 110567, 2023. https://doi.org/10.1016/j.compositesb.2023.110567

[5] MacAdams, L.A. and Kohli, D.K., "Bonding of composite materials," US 2016/0121591 A1, *United States Patent and Trademark Office*, May 5, 2016.

[6] MacAdams, L., and Kohli, D. "Development of a new bonding technology to create reliable nonds. Fuseply™, Part 1," *SAMPE Technical Conference Proceedings*, Long Beach, CA, May 21-24, 2018.

[7] Hudson, T.B., Follis, P.J., Pinakidis, J.J., Sreekantamurthy, T., and Palmieri, F.L., "Porosity detection and localization during composite cure inside an autoclave using ultrasonic inspection," *Composites Part A: Applied Science and Manufacturing*, Vol. 147, 106337, 2021. https://doi.org/10.1016/j.compositesa.2021.106337

[8] Hudson, T.B., Palmieri, F.L., Abbott, T.B., Seebo, J.P. and Burke, E.R., "Design of an automated ultrasonic scanning system for in-situ composite cure monitoring and defect detection," *SAMPE Technical Conference Proceedings*, Charlotte, NC, 2019. https://doi.org/10.33599/nasampe/s.19.1523

[9] Hudson, T.B., Serrano, K.M., Amador, A., Abbott, T.B., and Palmieri, F.L., "In-process ultrasonic cure monitoring system for defect detection and localization in composites," *SAMPE neXus Technical Conference Proceedings*, Virtual Event, June 29-July 1, 2021. https://www.digitallibrarynasampe.org/data/pdfs/s2021_pdfs/TP21-0000000599.pdf

[10] Davis, L.W., Day, R.J., Bond, D., Neesbitt, A., Ellis, J., and Gardon, E., "Effect of cure cycle heat transfer rates on the physical and mechanical properties of an epoxy matrix composite," *Composites Science and Technology*, Vol. 67(9), pp. 1892-1899, 2006. https://doi.org/10.1016/j.compscitech.2006.10.014

[11] Zhang, J., Xu, Y. C., and Huang, P., "Effect of cure cycle on curing process and hardness for epoxy resin," *Express Polymer Letters*, Vol. 3(9), pp. 534-541, 2009. https://doi.org/10.3144/EXPRESSPOLYMLETT.2009.67
[12] Czaderski, C., Martinelli, E., Michels, J., and Motavelli, M., "Effect of curing conditioned on strength development in an epoxy resin for structural strenghning," *Composites Part B*, Vol. 43(2), pp. 398-410, 2012. https://doi.org/10.1016/j.compositesb.2011.07.006
[13] Lapique, F., and Redford, K., "Curing effects on viscosity and mechanical properties of a commercial epoxy resin adhesive," *International Journal of Adhesion and Adhesives*, Vol. 22(4), pp. 337-346, 2002. https://doi.org/10.1016/S0143-7496(02)00013-1
[14] ASTM D7905/D7905M, "Standard test method for determination of the mode II interlaminar fracture toughness of unidirectional fiber-reinforced polymer matrix composites," *ASTM Standard*, 2014.
[15] O'Brien, T.K., Johnston W.M., and Toland, G.J., "Mode II interlaminar fracture toughness and fatique characterization of a graphite epoxy composite material," NASA/TM-2010-216838. https://ntrs.nasa.gov/citations/20100031113
[16] Jeong, H., "Effects of voids on the mechanical strength and ultrasonic attenuation of laminated composites," *Journal of Composite Materials*, Vol. 31(3), pp. 276-292, 1997. https://doi.org/10.1177/002199839703100303

VIII. Appendix

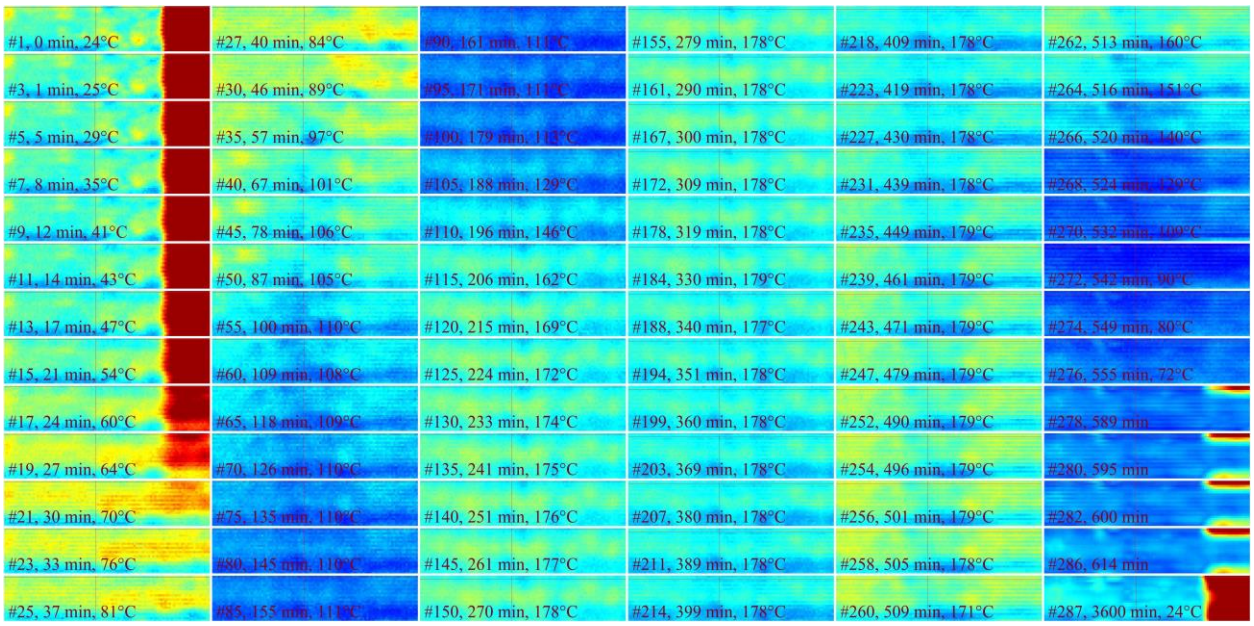

Fig. 12: Panel 1A C-scan images of the maximum amplitude measured at the AERoBOND joint line throughout the cure cycle.

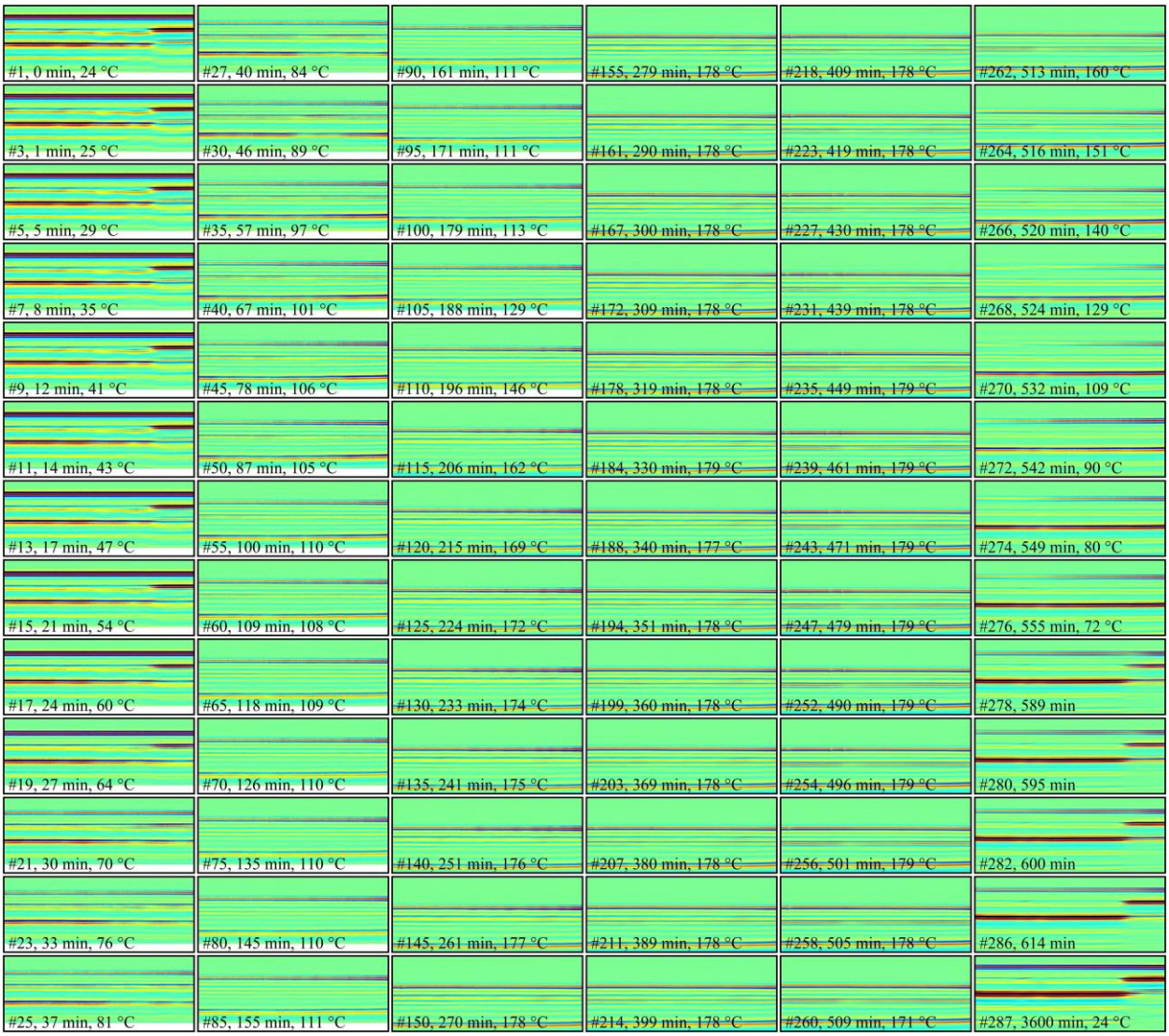

Fig. 13: B-scan images at one *y*-location throughout the cure cycle for Panel 1A.

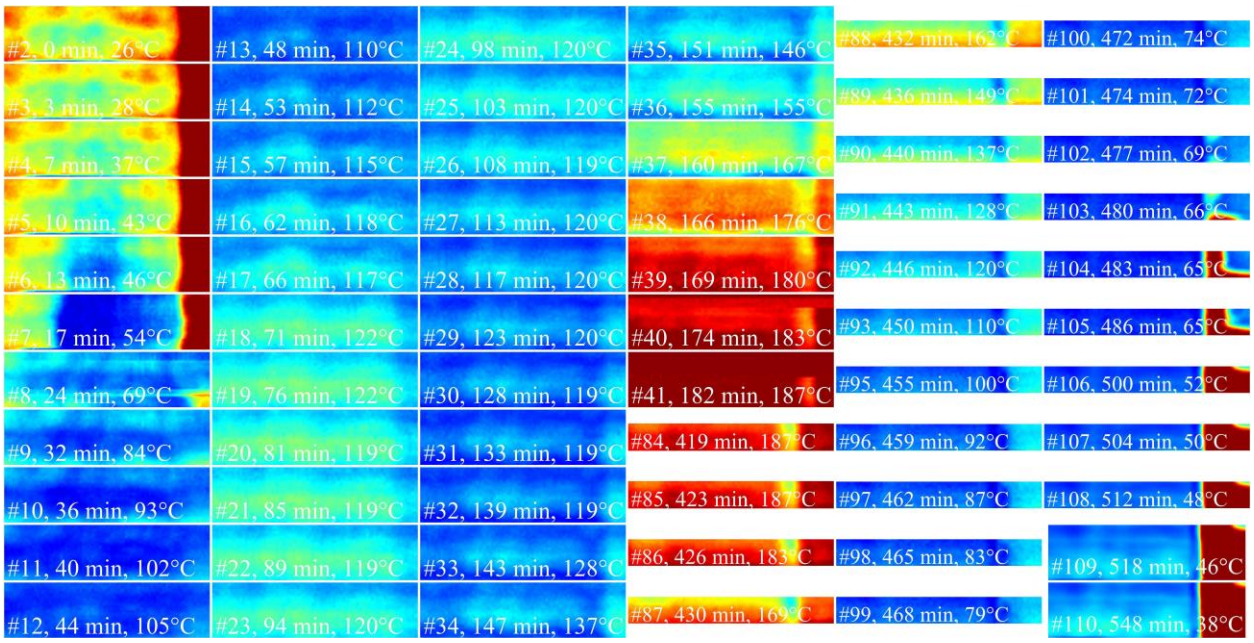

Fig. 14: Panel 3A C-scan images of the maximum amplitude measured at the AERoBOND joint line throughout the cure cycle.

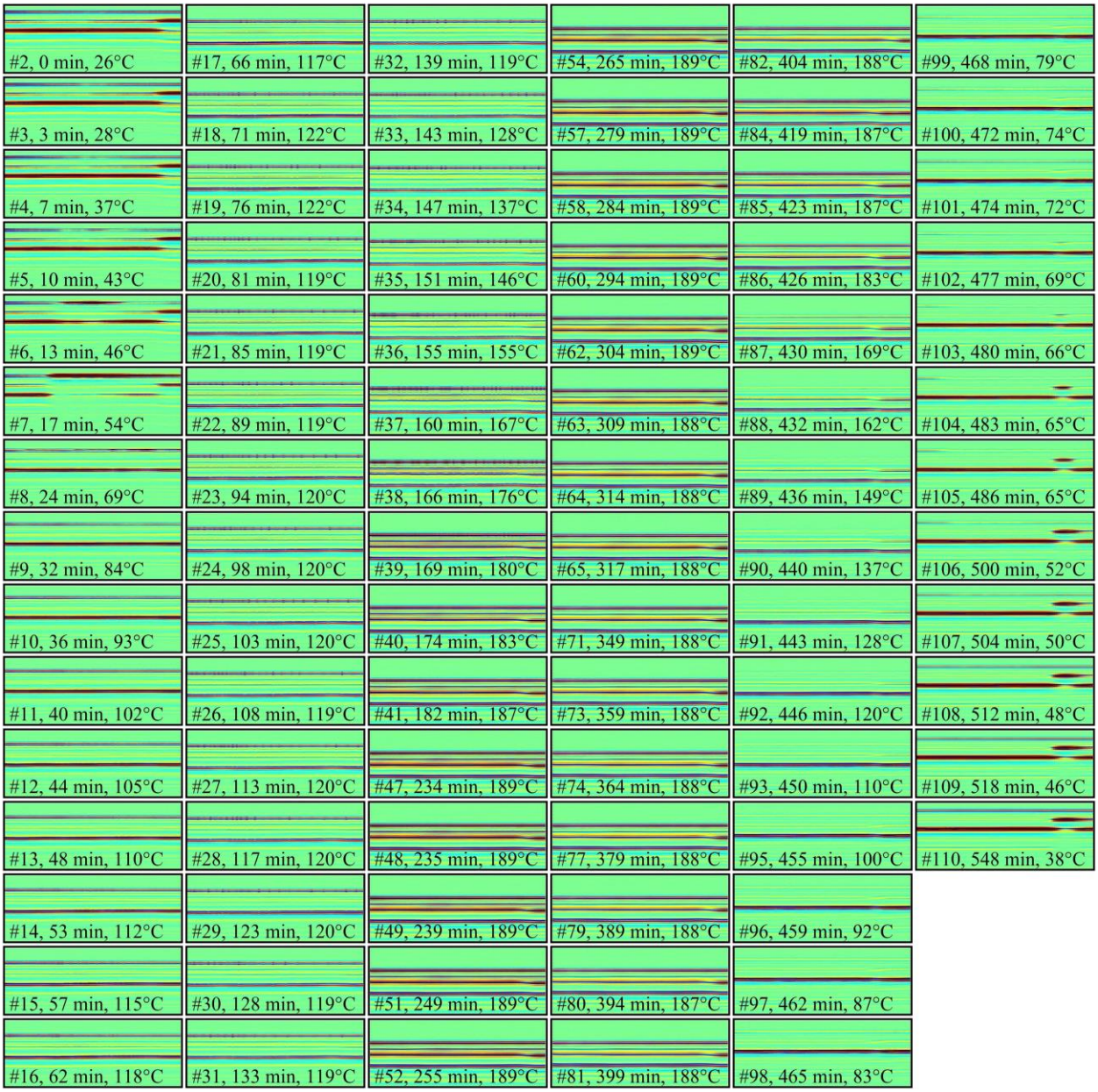

Fig. 15: B-scan images at one *y*-location throughout the cure cycle for Panel 3A.